Volume 1 | Number 1 | Jan 2013 | Pages 1–100

Nanoscale

www.rsc.org/nanoscale

ROYAL SOCIETY OF CHEMISTRY

ROYAL SOCIETY OF CHEMISTRY

www.rsc.org/nanoscale

Journal Name

ARTICLE TYPE

3-D TiO₂ Nanoparticle/ ITO Nanowire Nanocomposite Antenna for Efficient Charge Collection in Solid State Dye-sensitized Solar Cells

Gill Sang Han[a], Sangwook Lee[b], Jun Hong Noh[c], Hyun Suk Chung[a], Jong Hun Park[d], Bhabani Sankar Swain[a], Jeong-Hyeok Im[e], Nam-Gyu Park[e] and Hyun Suk Jung*[a]

TiO₂ nanoparticle (NP)/ITO nanowire (NW) nanocomposites for use as photoelectrode materials were fabricated to improve the charge collection efficiency in solid state dye sensitized solar cells (ss-DSSCs). The average current density for ss-DSSCs containing TiO₂ NP/ITO NW arrays was 7.2 mA/cm² that was ₁₀ 98% higher than that for the conventional TiO₂ NP ss-DSSCs. The intensity modulated photocurrent spectroscopy (IMPS) and intensity modulated photovoltage spectroscopy (IMVS) studies exhibited that the electron diffusion length of TiO₂ NP/ITO-NW nanocomposite ss-DSSCs was in the range of 4.3 ~ 5.6 μm, longer than that of TiO₂ NP solar cells (2.6 ~ 4.1 μm). The longer diffusion length was responsible for the boosted current densities of TiO₂ NP/ITO NW nanocomposite ss-DSSCs. We also employed the ₁₅ TiO₂ NP/ITO NW nanocomposite photoelectrode to inorganic-organic perovskite solar cell whose energy conversion efficiency was 7.5 %.

Introduction

Dye-sensitized solar cells (DSSCs) have received a vast amount of interest as promising alternative photovoltaic devices due to ₂₀ their relatively high efficiency and low production cost.[1] DSSCs have achieved energy conversion efficiency of 12.3 % using a zinc porphyrin dye sensitized TiO₂ nanoparticle (NP) films.[2,3] Solid-state dye-sensitized solar cells (ss-DSSCs) have generated a strong interest owing to problem of liquid electrolyte DSSCs ₂₅ which have suffered from electrolyte leakage and corrosion problem.[4] Moreover, ss-DSSCs have many advantages; mechanical and chemical stability with organic hole transporting materials (HTM), easy film formation and adjustable functionality by molecular design.[5] ss-DSSCs has exhibited ₃₀ energy conversion efficiency ~5% by using (2,2',7,7'-tetrakis (N,N-di-p-methoxyphenylamine)-9-9'-spiro-bifluorene (Spiro-OMeTAD) as the HTM.[6] Despite of these advantages, ss-DSSCs still have a low efficiency due to insufficient light harvesting limited by TiO₂ NPs films thickness. The electron diffusion ₃₅ length of TiO₂ was reported 4.4 μm in ss-DSSCs, but so far the highest efficiency of ss-DSSC is obtained for approximately 2 μm thickness of the mesoporous TiO₂ films.[7] This thickness is not sufficient to perfectly catch the incident photons, thereby deteriorating light harvesting efficiency. There have been several ₄₀ reports in order to increase light harvesting property of thin TiO₂ film. One is increasing of the molar extinction coefficient of dye molecules, which enhances the absorbance of solar spectrum with thin TiO₂ film.[8-10] Second, is to increase the surface area of thin TiO₂ film for enhancing the amount of dye loading.[11-13] The ₄₅ simplest way to enhance light harvesting property is to increase the TiO₂ NP film thickness. However, the limitation of charge collection capability restricts the film thickness. Therefore, many

studies have previously focused on replacing TiO₂ NP film with one-dimensional (1-D) nanostructures, such as TiO₂ nanowire, ₅₀ nanorods and nanotubes to provide unidirectional conduction pathway for enhancing charge collection of photoelectrode.[14-18] However, these 1-D materials don't have enough surface area to adsorb large amount of dye molecules, which is another bottle neck for achieving high efficiency. For this reason, 3-D ₅₅ nanostructure photoelectrode containing mixture of 1-D nanomaterials and 0-D nanoparticles is an alternative to improve the charge collection as well as to ensure high surface area.

In the present study, we fabricated a 3-D TiO₂ NP/ITO NW nanocomposite for use as a photoelectrode material in ss-DSSC, ₆₀ whose photocurrent density was 98% higher than TiO₂ NP ss-DSSC due to superior charge collection capability. Moreover, we also applied the same concept to inorganic-organic hybrid Perovskite solar cell and achieved 7.5 % efficiency.

Experimental

Synthesis of ITO Nanowire Arrays

₆₅ ITO NW arrays were synthesized by vapour transport method.[19] Au seeds were deposited on ITO glass by using an ion beam coater (Eiko-IB-3). To fabricate ITO NWs, Au coated ITO glass was placed at the outlet of tube furnace. Mixture of Indium and ₇₀ tin metal powder of an atomic ratio of 3:1, was placed at the centre of the quartz tube in tube furnace. The furnace was taken into vacuum condition under 1.0 mTorr by rotary pump. Then, the tube furnace was heated to 850 °C at a rate of 10 °C min⁻¹. Oxygen gas was disembogued with flow rate of 12 standard cubic ₇₅ centimetres per second (sccm) into tube furnace during the growth of ITO NWs.
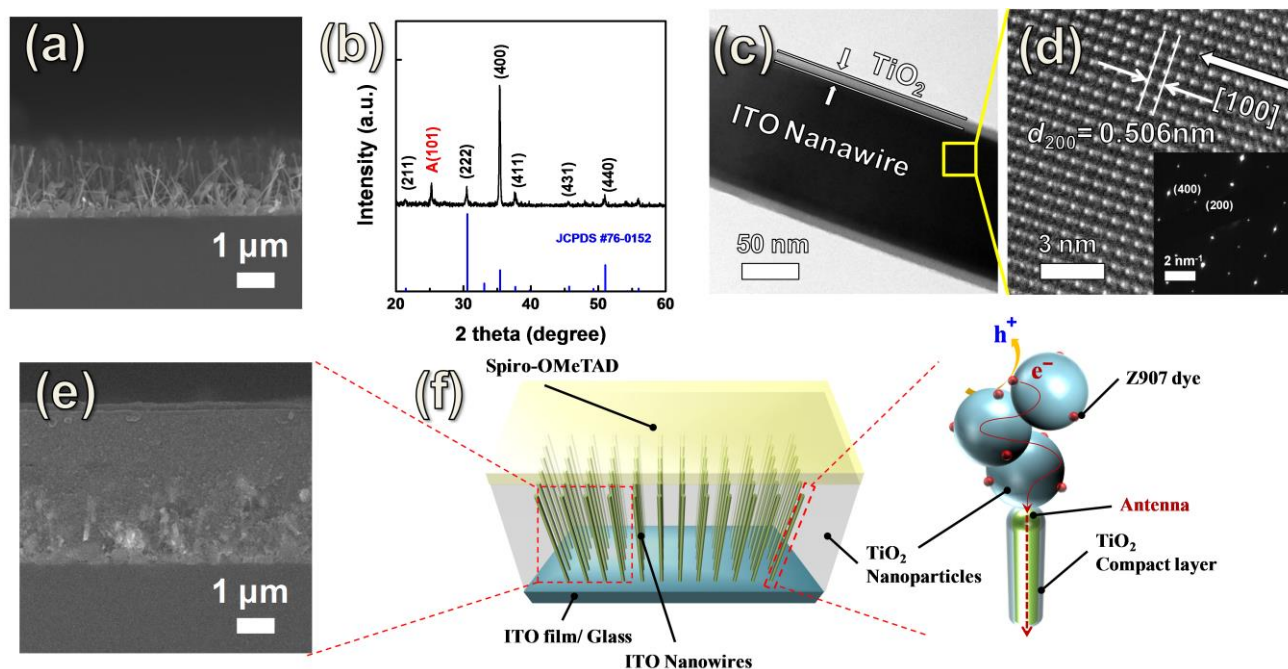
Fig. 1 (a) SEM image of synthesized ITO nanowire arrays, (b) X-ray diffraction patterns of TiO$_2$ deposited ITO nanowire arrays by ALD, (c) TEM image of TiO$_2$ deposited ITO nanowire, (d) High-resolution TEM image of ITO nanowire and inset is a selective area electron diffraction pattern, (e) SEM image of TiO$_2$ NP/ ITO NW nanocomposite photoelectrode, (f) Scheme of TiO$_2$ NP/ ITO NW nanocomposite ss-DSSCs.

Fabrication of solar cells

To fabricate ITO NW ss-DSSCs, the ITO NWs were coated with ~10 nm TiO$_2$ thin layers by using atomic layer deposition (ALD). The deposition was performed at 300 °C using the plasma. TiO$_2$
5 NP/ ITO NWs nanocomposite was fabricated by spin coating method, which filled ~20 nm anatase TiO$_2$ NPs into ITO NW arrays. Then, TiO$_2$ NPs/ITO NWs nanocomposite were annealed at 450 °C in an air atmosphere for 1h followed by Z907 dye loading in a 5 × 10^{-4} M solution of acetonitrile:t-butanol (1:1) for
10 8h. The hole transport materials (HTM) was synthesized with dissolving the spiro-OMeTAD (2,2'7,7'-tetrakis-(N,N-dipmethoxyphenylamine) 9,9'-spirobifluorene) in chlorobenzene (0.17 M) containing tert-butylpyridine (TBP) and lithium-bis (trifluoromethanesulphonyl) imide (TFSI) additives. HTM was
15 deposited on the TiO$_2$ NPs/ITO NWs nanocomposite by spin-coating at 2000 rpm for 40 s. Finally, 80 nm thick Ag electrodes were deposited on HTM layers by using thermal evaporation.

Fabrication of CH$_3$NH$_3$PbI$_3$ perovskite solar cells

To verify the effect of TiO$_2$ NPs/ITO NWs arrays on perovskite
20 solar cell, we also fabricated the perovskite solar cell using the same concept. The CH$_3$NH$_3$PbI$_3$ was synthesized by process reported earlier.[20] The methyl ammonium iodide was synthesized as follows; hydroiodic acid (30 mL, 0.227 mol, 57 wt. % in water) and methylamine (27.8 mL, 0.273 mol, 40 % in methanol) were
25 stirred on the round bottom flask at 0 °C for 2 h. The solution was evaporated to precipitate the white powder (CH$_3$NH$_3$I). The CH$_3$NH$_3$I was washed three times in diethyl ether and dried in vacuum oven at 60 °C for 6h. To synthesize CH$_3$NH$_3$PbI$_3$, PbI$_2$

(1.3 M) in γ-butyrolactone (2 ml) was added into the CH$_3$NH$_3$I
30 solution (1.3 M) dissolved in γ-butyrolactone at 60 °C followed by stirring the solution overnight. The CH$_3$NH$_3$PbI$_3$ layer was deposited on the TiO$_2$ NPs/ITO NWs nanocomposite substrate using a spin-coating method. It was followed by heating at 100 °C for 15 min. Finally, HTM and Ag electrode were deposited in the
35 same manner as discussed in the above section.

Characterization

The morphology of the ITO NW arrays was observed by a field-emission scanning electron microscopy (FESEM, JSM-7600F, JEOL). The crystal structure and phase analysis of the ITO NWs
40 array were analyzed by X-ray diffractometer (XRD, D-MAX 2500, Rigaku) with CuKα radiation. Furthermore, the ITO NWs were investigated by high-resolution transmission electron microscopy (HR-TEM, JEM-3000F, JEOL). Photovoltaic properties were measured by using a potentiostat (CHI660, CHI
45 instrument) and solar simulator (Oriel Sol 3A class AAA, Newport). Optical absorbance spectra were recorded by a UV–Vis spectrometer (Lamda 35, Perkin-Elmer). The amount of dye molecules were determined by the desorbed dye in an alkaline alcoholic solution. The electron transport and recombination time
50 were measured by intensity modulated photocurrent spectroscopy (IMPS) and intensity modulated photovoltage spectroscopy (IMVS) (Zahner, Zennium) with a red light-emitting diode (627 nm). The incident photon to current conversion efficiency was measured with IPCE measurement system (PV Measurements).

55 ## Results and discussion
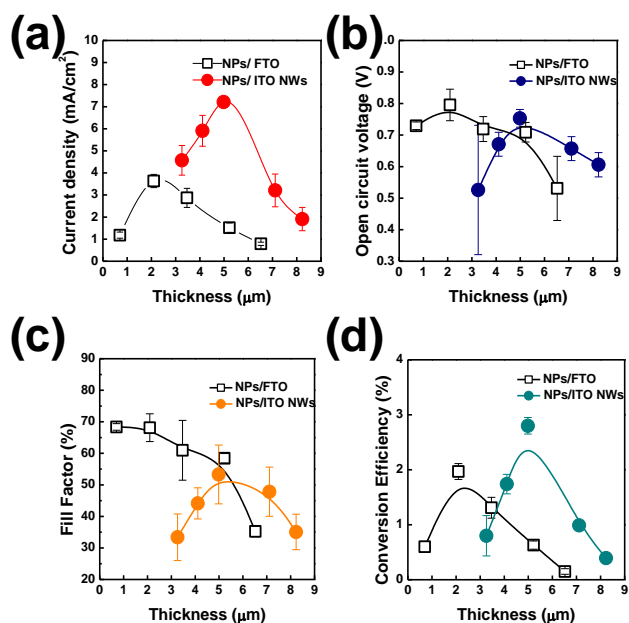
Fig. 2 Photovoltaic properties of TiO$_2$ NP and TiO$_2$ NP/ITO NW nanocomposite ss-DSSCs (a) photocurrent density, (b) open circuit voltage, (c) fill factor, and (d) power conversion efficiency as a function of active layer thickness, respectively.

Indium tin oxide (ITO) nanowires (NWs) were grown by vapor-liquid-solid (VLS) method using Au catalysts on glass substrate. Fig. 1 (a) shows the FE-SEM image of ITO nanowires (NWs) grown on the ITO/glass substrate. The length of aligned ITO
5 NWs is about 2 μm and diameter is about 70 nm. Fig. 1 (b) shows the X-ray diffraction (XRD) pattern of ITO NW array which is consistent with cubic In$_2$O$_3$ (JCPDS #76-0152). The electrical resistivity of the ITO NW array was 4.7 × 10^{-4} Ωcm, in good agreement with the previous results.[19] Given that relative
10 intensity of (400) peak is much stronger than (222) peak for ITO NW arrays, ITO NWs are grown along with [100] direction.
For application of ITO NW to ss-DSSC, TiO$_2$ thin layer with about 20 nm thicknesses was deposited on ITO NWs using a plasma-enhanced atomic layer deposition (PEALD). Fig. 1 (c)
15 shows HRTEM image of a TiO$_2$ coated ITO NW, which demonstrates a conformal TiO$_2$ coating on ITO NW. The TiO$_2$ thin layer was found to be anatase phase, optimized from our previous report.[21] Fig. 1 (d) shows the HRTEM image of ITO NW. The lattice image with a d-spacing of 0.51 nm for (200),
20 consistent with the lattice parameter of cubic In$_2$O$_3$. The selective area electron diffraction (SAED) patterns of ITO NW clearly shows that ITO NW is single crystalline and grown along the [100] direction (Inset of Fig. 1 (d)). To increase the surface area of ITO NW-based photoelectrode, TiO$_2$ colloid penetrated into
25 ITO NW array using a spin-coating method. Fig. 1 (e) presents FESEM image of TiO$_2$ NP/ITO NW nanocomposite photoelectrode containing 20 nm TiO$_2$ NPs and 2.1 μm long ITO NWs. The thickness of TiO$_2$ NP/ITO NW nanocomposites was varied by changing number of spin coating, presented in
30 supplementary information 1. As illustrated in Fig. 1 (f), the generated electrons are expected to be easily captured by ITO NWs which are able to play role of antennas.
Fig. 2 shows the photovoltaic (PV) properties of TiO$_2$ NP/ITO
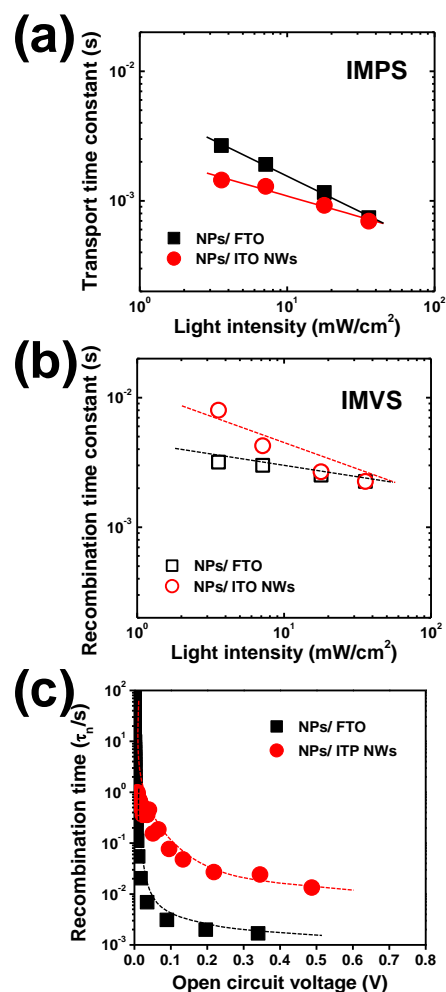
Fig. 3 Charge transport properties of TiO$_2$ NP (black line, 4.5 μm) and TiO$_2$ NP/ ITO NW nanocomposite ss-DSSCs (red line, 4.8 μm); (a) intensity modulated photocurrent spectroscopy, (b) intensity modulated photovoltage spectroscopy, and (c) recombination time obtained from the transient V$_{oc}$ study.

NW nanocomposite ss-DSSCs compared with conventional TiO$_2$
35 NP ss-DSSCs. More information of variation of PV properties as a function of active layer thickness is presented in supplementary information 2. As shown in Fig. 2(a), the photocurrent density for the TiO$_2$ NP/ ITO NW nanocomposite ss-DSSCs is dramatically increased from average current density 4.5 mA/cm^2 at
40 approximately 3.2 μm to 7.2 mA/cm^2 at 4.8 μm thickness. In contrast, maximum photocurrent density for TiO$_2$ NP ss-DSSC is 3.6 mA/cm^2 at 2.1 μm thickness. The photocurrent density for TiO$_2$ NP/ITO NW nanocomposite photoelectrode with an optimal thickness of 4.8 μm is approximately 98% higher than that for
45 TiO$_2$ NP photoelectrode with an optimal thickness of 2.1 μm. Over the same thickness range, the open circuit voltage (V_{oc}) shows the similar trend with photocurrent density. The maximum V_{oc} of TiO$_2$ NP ss-DSSC is approximately 800 mV (2.1 μm). In the case of TiO$_2$ NP/ITO NW nanocomposite ss-DSSCs, V_{oc}
50 increases from 530 mV (3.2 μm) to 750 mV (4.8 μm), and then the V_{oc} is decreased. This trend is related to quasi-Fermi level and charge recombination. In the regime of thinner thickness, the concentration of photoelectrons is not sufficient to increase quasi-
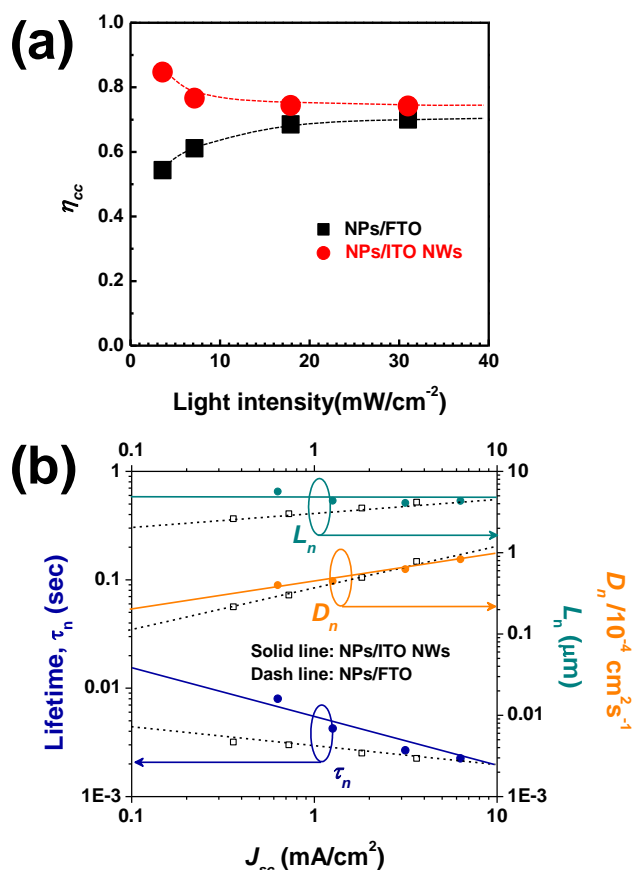
Fig.4 (a) Charge collection efficiency and (b) electron lifetimes, diffusion coefficients and electron diffusion lengths of the TiO_2 NP (black line, 4.5 μm) and TiO_2 NP/ ITO NW nanocomposite ss-DSSCs (4.8 μm)

Fermi level enough to reach high V_{oc}. Over maximum V_{oc}, the concentration of photoelectrons is too high, which is a driving force for charge recombination. Also, the film thickness is too thick to collect all of photoelectrons due to the limitation on electron diffusion length.[7] The nanocomposite ss-DSSCs exhibit lower fill factors than the TiO_2 NP ss-DSSCs in the overall thickness range, ascribed to the deterioration of sheet resistance of ITO films after 450 °C heat-treatment. The original sheet resistance of ITO film is approximately 10 Ω/□. Further heat-treatment for the fabrication of photoelectrodes increases the sheet resistance by 40 Ω/□, which is consistent with our previous results.[22] The deteriorated conductivity of ITO films increases the series resistance, consequently reducing the fill factor. In contrast, the TiO_2 NP ss-DSSCs employ the FTO films whose sheet resistance does not change after the same heat-treatment process.

The J–V characteristic of the best-performing cell is presented in supplementary information 3. In case of the TiO_2 NP ss-DSSC under an irradiance of AM 1.5 conditions, we achieved the values of 3.82 $mAcm^{-2}$, 820 mV, 0.69 and 2.17 % for J_{sc}, V_{oc}, fill factor (ff), and the power conversion efficiency (PCE), respectively. On the other hand, TiO_2 NP/ITO NW nanocomposite ss-DSSC shows the respective value of 6.30 $mAcm^{-2}$, 774 mV, 0.61 and 3.0%, respectively. The PCE of TiO_2 NP/ITO NWs nanocomposite ss-DSSC (4.8 μm) is about 40 % higher than the TiO_2 NP ss-DSSC (2.1 μm).

To understand the difference in the photovoltaic performance of TiO_2 NP/ITO NW nanocomposite ss-DSSC compared to TiO_2 NP ss-DSSC, the charge collection properties were investigated by analyzing intensity modulated photocurrent spectroscopy (IMPS), intensity modulated photovoltage spectroscopy (IMVS) and transient open circuit voltages. To improve reliability of this analysis, the thickness of TiO_2 NP/ITO NW nanocomposite and TiO_2 NP photoelectrodes were fixed at 4.8 μm and 4.5 μm, respectively. As presented in supplementary information 4, the amount of dye adsorption is similar with each other at this thickness, implying that the number of photoelectrons are similar. The IMPS is related to photoelectron transport time through the photoelectrode under short-circuit condition, and the IMVS provides the information about recombination time that the electrons generated from dyes and holes in HTM recombine under open circuit voltage condition.[23] Fig 3(a) and (b) show the IMVS and IMVS data as function of light intensity, respectively. The results show the TiO_2 NP/ITO NW nanocomposite ss-DSSC has faster charge transport time (τ_c) and longer recombination time (τ_r) than TiO_2 NP ss-DSSC. Moreover, the transient V_{oc} data which is another way to characterize the charge recombination time also support to our result. The apparent recombination time of the photoelectrons can be evaluated by the following expression [24]:

$$\tau_n = -\frac{k_B T}{e}\left(\frac{dV}{dt}\right)^{-1} \tag{1}$$

Where k_B is the Boltzmann constant and T is the temperature. Therefore, Fig 3(c) shows the electron recombination time of TiO_2 NP/ITO NW nanocomposite ss-DSSC (red line), which is about 1 order longer than TiO_2 NP ss-DSSCs (black line).

The superior photovoltaic performance for the TiO_2 NP/ITO NW nanocomposite ss-DSSC, i.e. the higher photocurrent, would be attributed to several parameters. Photocurrent is in proportion to product of light harvesting efficiency (η_{lh}), electron injection efficiency (η_{inj}), and charge collection efficiency (η_{cc}), expressed as follows.[17]

$$J_{sc} \propto \eta_{lh}\eta_{inj}\eta_{cc} \tag{2}$$

The light-harvesting property is directly related to the degree of dye loading. As aforementioned, these samples possessed similar amount of dye adsorptions, which indicates that both ss-DSSCs should exhibit similar light harvesting property. Moreover, the electron injection efficiency can be ignored because of employing the same dye molecules (Z907 dye) and TiO_2 nanoparticles.[12,25] Therefore, higher photocurrent of TiO_2 NP/ITO NW nanocomposite ss-DSSC is probably attributed to excellent charge collection efficiency.

As plotted in Fig. 4(a), the charge collection efficiency was calculated from following expression[17]:

$$\eta_{cc} \equiv 1 - \frac{\tau_e}{\tau_r} \tag{3}$$

TiO_2 NP/ITO NW nanocomposite ss-DSSC has higher charge collection efficiency (Max.; ~0.85) than TiO_2 NP ss-DSSC (Max.; ~0.7) over all light intensity range. These results originate from the fast charge transport time and longer recombination time, which ultimately increase the electron diffusion length. Fig. 4(b)
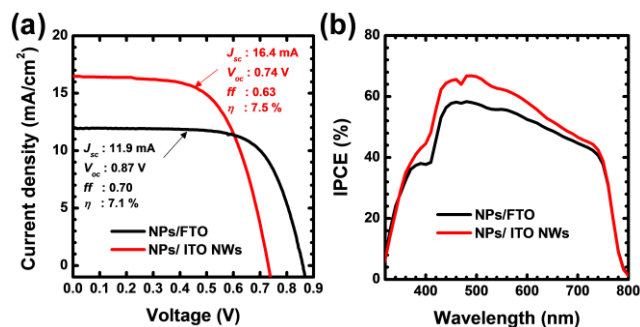
Fig. 5 (a) Photovoltaic *J-V* curves, (b) IPCE spectra of TiO$_2$ NP/ ITO NW nanocomposite and TiO$_2$ NP CH$_3$NH$_3$PbI$_3$ perovskite solar cell.

shows the electron diffusion length (L_n), electron diffusion coefficient (D_n), and electron life time (τ_n) with respect to short circuit current (J_{sc}). Electron diffusion length is given by $L_n = (D\tau)^{1/2}$, where D and τ are the diffusion coefficient and the life time of electrons, respectively. Electron diffusion length of TiO$_2$ NP ss-DSSC is in the range of 2.6 ~ 4.1 μm, consistent with already reported values.[7] The TiO$_2$ NP/ITO NW nanocomposite ss-DSSCs exhibit the longer electron diffusion length, 4.3 ~ 5.6 μm, which enables to collect electrons that are generated at a deeper region. This is a reason why the TiO$_2$ NP/ITO NW nanocomposite photoelectrode is capable of generating higher photocurrent by increasing the optimized thickness to 4.8 μm. At this thickness, the amount of dye loading for the TiO$_2$ NP/ITO NW nanocomposite photoelectrode is 1.8 times higher than that for the TiO$_2$ NP photoelectrode with the optimized thickness of 2.1 μm, which consequently yields 98% higher photocurrent density for the TiO$_2$ NP/ITO NW nanocomposite ss-DSSCs.

To demonstrate the same effect of TiO$_2$ NP/ITO NW nanocomposite photoelectrode on inorganic-organic hybrid solar cell, we employed the perovskite CH$_3$NH$_3$PbI$_3$ absorber instead of Z907 dye. Perovskite CH$_3$NH$_3$PbI$_3$ absorber has a long absorption range and high absorption coefficient, which is recently an emerging solar cell material. We fabricated TiO$_2$ NP/ITO NW nanocomposite and TiO$_2$ NP photoelectrodes with thickness of 900 and 500 nm, respectively. The thickness for each solar cell was optimized to perform the best photovoltaic property under same condition. Fig. 5 shows the PV properties of TiO$_2$ NP/ITO NW nanocomposite and TiO$_2$ NP perovskite solar cell. In case of the TiO$_2$ NP perovskite solar cells, the typical photovoltaic characteristics are 11.9 mAcm^{-2}, 0.87 V, 0.70 and 7.1 % for J_{sc}, V_{oc}, fill factor (*ff*), and the PCE, respectively. The TiO$_2$ NP/ITO NW nanocomposite perovskite solar cell shows the respective value of 16.4 mAcm^{-2}, 0.74 V, 0.63 and 7.5 %. The photocurrent density for the nanocomposite perovskite solar cell is approximately 40 % higher than TiO$_2$ NP perovskite solar cell. Also, the incident photon to current conversion efficiency (IPCE) for the nanocomposite perovskite solar cell is higher than TiO$_2$ NP one in the overall wavelength. These results demonstrate the superior charge collection properties of TiO$_2$ NP/ITO NWs nanocomposite materials and their potentials for use as an efficient charge collector in the perovskite solar cells.

Conclusions

In summary, we synthesized single crystalline ITO NW arrays oriented along [100] direction and fabricated TiO$_2$ NP/ITO NW nanocomposite for use as photoelectrode materials in ss-DSSCs. TiO$_2$ NP/ITO NW nanocomposite ss-DSSC has higher charge collection efficiency as well as longer diffusion length compared with conventional TiO$_2$ NP ss-DSSC. The superior charge collection property of ITO NW enabled to increase the thickness of photoelctrode to 4.8 μm, yielding 98% higher photocurrent than TiO$_2$ NP ss-DSSC. We also employed the TiO$_2$ NP/ITO NW nanocomposite in perovskite CH$_3$NH$_3$PbI$_3$ solar cells, which exhibited the power conversion efficiency (PCE) of 7.5%. Our study demonstrates that superior charge collection capability for TiO$_2$ NP/ITO NW nanocomposite materials can make it viable to boost up energy conversion efficiency of photo-energy conversion devices such as ss-DSSCs, quantum dot solar cells, and water-splitting photochemical cells.

Acknowledgements

Notes

[a] *School of Advanced Materials Science & Engineering, Sungkyunkwan University, Suwon, 440-746, Korea. Fax: +82-31-290-7410; Tel: +82-31-290-7403; E-mail:hsjung1@skku.edu.*
[b] *Department of Material Science and Engineering, University of California at Berkeley, CA94709, USA.*
[c] *KRICT-EPFL Global Research Laboratory, Advanced Materials Division, Korea Research Institute of Chemical Technology, Daejeon, 305-600, Korea.*
[d] *Department of Materials Science and Engineering, Seoul National University, Seoul, 151-744, Korea*
[e] *School of Chemical Engineering and Department of Energy Science, Sungkyunkwan University, Suwon, 440-746, Korea.*
† Electronic Supplementary Information (ESI) available: SEM images of 3-D TiO$_2$ nanoparticle (NP) /ITO nanowire (NW) nanocomposite photoelectrode, photovoltaic properties, *J-V* curves for the best performance cells, and plot of dye loading vs. active layer thickness. See DOI: 10.1039/b000000x/

References

1 B. O'regan and M. Grätzel, *Nature*, 1991, **353**, 737.
2 A. Yella, H. W. Lee, H. N. Tsao, C. Y. Yi, A. K. Chandiran, M. K. Nazeeruddin, E. W. G. Diau, C. Y. Yeh, S. M. Zakeeruddin, and M. Grätzel, *Science,* 2011, **334**, 629
3 H. S. Jung and J. K. Lee, *J. Phys. Chem. Lett.*, 2013, **4**, 1682.
4 H. J. Snaith and L. Schmidt-Mende, *Advanced Materials*, 2007, **19**, 3187.
5 U. Bach, D. Lupo, P. Comte, J. E.Moser, F. Weissörtel, J. Salbeck, H. Spreitzer and M. Grätzel, *Nature*, 1998, **395**, 583.
6 H. J. Snaith, A. J. Moule, C. Klein, K. Meerholz, R. H. Friend, and M. Grätzel, *Nano Letters*, 2007, **7**, 3372.
7 J. Kruger, R. Plass, M. Grätzel, P. J. Cameron, L. M. Peter, *J. Phys. Chem. B*, 2003, **107**, 7536
8 K. Hara, Z. -S. Wang, T. Sato, A. Furube, R. Katoh, H. Sugihara, Y. Dan-oh, C. Kasada, A. Shinpo, and S. Suga, *J. Phys. Chem. B*, 2005, **109**, 15476.

9 F. Gao, Y. Wang, D. Shi, J. Zhang, M. Wang, X. Jing, R. Humphry-Baker, P. Wang, S. M. Zakeeruddin and M. Grätzel, *J. Am. Chem. Soc.*, 2008, **130**, 10720.

10 H. Choi, I. Raabe, D. Kim, F. Teocoli, C. Kim, K. Song, J. -H. Yum, J. Ko, M. K. Nazeeruddin, and M. Grätzel, *Chemistry - A European Journal*, 2010, **16**, 1193.

11 J. Bisquert, D. Cahen, G. Hodes, S. Rühle and A. Zaban, *J. Phys. Chem. B*, 2004, **108**, 8106.

12 M. Grätzel, *Inorganic Chemistry*, 2005, **44**, 6841.

13 D. Chen, F. Huang, Y. Cheng, R. A. Caruso, *Advanced Materials*, 2009, **21**, 2206.

14 M. Law, L. E. Greene, J. C. Johnson, R. Saykally and P. Yang, *Nature Materials*, 2005, **4**, 455.

15 J. Y. Kim, S. B. Choi, D. W. Kim, S. W. Lee, H. S. Jung, J. -K. Lee and K. S. Hong, *Langmuir*, 2008, **24**, 4316.

16 M. Wang, J. Bai, F. L. Formal, S. -J. Moon, L. Cevey-Ha, R. Humphry-Baker, C. Grätzel, S. M. Zakeeruddin and Michael Grätzel, *J. Phys. Chem. C*, 2012, **116**, 3266

17 K. Zhu, N. R. Neale, A. Miedaner and A. J. Frank, *Nano Letters*, 2007, **7**, 69.

18 S. Lee, I. J. Park, D. H. Kim, W. M. Seong, D. W. Kim, G. S. Han, J. Y. Kim, H. S. Jung and K. S. Hong, *Energy Environ. Sci.*, 2012, **5**, 7989

19 J. H. Noh, H. S. Han, S. Lee, J. Y. Kim, K. S. Hong, G. S. Han, H. Shin and H. S. Jung, *Adv. Energy Mater.*, 2011, **1**, 829.

20 H. -S. Kim, C. -R. Lee, J. -H. Im, K. -B. Lee, T. Moehl, A. Marchioro, S. -J. Moon, R. Humphry-Baker, J. -H. Yum, J. E. Moser, M. Grätzel and N. -G. Park, *Scientific Reports*, 2012, **2** ,591.

21 H. S. Han, J. S. Kim, D. H. Kim, G. S. Han, H. S. Jung, J. H. Noh, K. S. Hong, *Nanoscale*, 2013, **5**, 3520

22 S. W. Lee, J. H. Noh, S. T. Bae, I. S. Cho, J. Y. Kim, H. H. Shin, J. K. Lee, H. S. Jung, K. S. Hong, *J. Phys. Chem. C*, 2008, **113**, 7443

23 J. R. Jennings and L. M. Peter, *J. Phys. Chem. C*, 2007, **111**, 16100.

24 J. Bisquert, A. Zaban, M. Greenshtein and I. Mora-Sero, *J. Am. Chem. Soc.*, 2004, **126**, 13550.

25 Y. Tachibana, J. E. Moser, M. Grätzel, D. R. Klug and J. R. Durrant, *J. Phys. Chem.*, 1996, **100**, 20056.

Nanoscale Accepted Manuscript